International Journal of Automotive Technology, Vol. 5, No. 4, pp. 257–268 (2004)

1229-9138/2004/018-04

WAVELET ANALYSIS OF VEHICLE NONSTATIONARY VIBRATION UNDER CORRELATED FOUR-WHEEL RANDOM EXCITATION

Y. S. WANG[1,2], C.-M. LEE[2)*] and L. J. ZHANG[1)]

[1)]Department of Automotive Engineering, Liaoning Institute of Technology, No. 169 Shiying Street, Guta District, Jinzhou, China
[2)]Department of Mechanical and Automotive Engineering, University of Ulsan, Ulsan 680-749, Korea

(Received 29 August 2003; Revised 23 August 2004)

ABSTRACT–The wavelet analysis method is introduced in this paper to study the nonstationary vibration of vehicles. A new road model, a so-called time domain correlated four-wheel road roughness, which considers the coherence relationships between the four wheels of a vehicle, has been newly developed. Based on a vehicle model with eight degrees of freedom, the analysis of nonstationary random vibration responses was carried out in a time domain on a computer. Verification of the simulation results show that the proposed road model is more accurate than previous ones and that the simulated responses are credible enough when compared with some references. Furthermore, by taking wavelet analysis on simulated signals, some substantial rules of vehicle nonstationary vibration, such as the relationship between each vibration level, and how the vibration energy flows on a time-frequency map, beyond those from conventional spectral analysis, were revealed, and these will be of much benefit to vehicle design.

KEY WORDS : Wavelet analysis, Time-frequency map, Vehicle nonstationary vibration, Correlated four-wheel random excitation.

NOMENCLATURE

m_B : mass of the vehicle body
J_y : pitch moment of inertia of the vehicle body
J_x : roll moment of inertia of the vehicle body
m_{fl} : left half mass of the front axle (including tyre)
m_{fr} : right half mass of the front axle (including tyre)
m_r : mass of the rear axle (including tyres)
J_{rq} : angle moment of inertia of the rear axle
m_s : mass of the human being and seat
k_{tf} : stiffness of a front tire
k_{tr} : stiffness of a rear tire
k_f : spring stiffness of the front suspension
k_r : spring stiffness of the rear suspension
k_s : stiffness of the seat
c_f : damping coefficient of the front suspension
c_r : damping coefficient of the rear suspension
c_s : damping coefficient of the seat
l_1 : horizontal distance from the m_B to the front axle
l_2 : horizontal distance from the m_B to the rear axle
l_3 : half distance between the two front springs
l_4 : longitudinal horizontal distance from the m_B to m_s
l_5 : half-distance between the two rear springs
l_6 : half-distance between the two front wheels
l_7 : transverse horizontal distance from the m_B to m_s
l_8 : half-distance between the two rear wheels
Z_B : vertical displacement of the vehicle body
θ_b : roll angle of the vehicle body
ϕ_B : pitch angle of the vehicle body
Z_s : vertical displacement of the m_s
Z_{fl} : vertical displacement of the m_{fl}
Z_{fr} : vertical displacement of the m_{fr}
Z_r : vertical displacement of the rear axle
θ_r : angular displacement of the rear axle

SUBSCRIPTS
L : left wheel
R : right wheel
f : front wheel
r : rear wheel

*Corresponding author. e-mail: cmlee@ulsan.ac.kr

1. INTRODUCTION

As the standard of living has been improving, people are more concerned about the ride comfort of their cars. To improve the ride comfort, a great deal of research on vehicle vibration systems including road roughness was issued from theory and experiment fields in the past few decades. Most of these research works were based on linear or nonlinear models such as SDOF and MDOF

with road excitations in terms of PSD (power spectral density) (Dodds *et al.*, 1973; Renucci *et al.*, 1976) or time course (Zhang, 1986; Wang and Wu, 1987; Yu and Guo, 1998), Some research involved the parameter optimization of passive suspension (Dokainish *et al.*, 1980; Hac, 1985; Shi *et al.*, 1995), and moreover, the active and semi-active suspension development (Thompson *et al.*, 1984; Haday *et al.*, 1989; Esmailzadeh *et al.*, 1997; Yu and Guo, 1998). It can be seen that most of the research mentioned above assumed that the vehicles were running at certain constant speeds, therefore, were regarded as a stationary random process. Actually, in more usual cases such as starting, accelerating and braking, vehicles work under variable speed conditions, and its vibration should be considered as a nonstationary process accordingly (Zhang *et al.*, 2002). Because of theory restriction, however, there are only a few of approaches to this topic that have been developed. In this paper, a new road-roughness model with four-wheel input was established and, furthermore, a set of methods for nonstationary vibration simulation was proposed, based on a full-vehicle model with eight degrees of freedom.

In the signal processing field, Fast Fourier Transform (FFT), a very effective approach for stationary signals, was widely used in vehicle engineering (Welch, 1967; Newland, 1984; Brigham, 1988). It can be utilized to extract time-averaged energy information from a signal segment with time length T only in frequency domain, but nothing remains in time domain. For nonstationary signals, both the frequencies and their magnitudes vary with time so that FFT cannot deal with them properly. To solve this problem, many time-frequency analysis (TFA) algorithms have been developed in recent years. Typical implementation examples are the short-time Fourier Transform (STFT) (Hodges *et al.*, 1985), Wigner-Ville distribution (WVD) and its improved version smoothed pseudo-Wigner-Ville distribution (SPWVD) (Baydar *et al.*, 2001), the wavelet transform (WT) (Daubechies, 1990), and so on. The advantages and drawbacks of these methods have also been discussed (Gade *et al.*, 1996). The WT as "Mathematical Microscope" in engineering (Chen, F. S., 1998) allows the changing spectral composition of a nonstationary signal to be measured and presented in the form of a time-frequency map and thus, was suggested as a tool for nonstationary vibration analysis (Newland *et al.*, 1994). Therefore, instead of the conventional FFT method, the Continuous Wavelet Transform (CWT) as well as the Discrete Wavelet Transform (DWT) were first applied to study the nonstationary inputs and responses of the vehicle vibration system in this paper, and some valuable conclusions beyond FFT are deduced from the time-frequency map.

2. SYSTEM MODELING

2.1. Modeling of the Vehicle Vibration System

This paper built a dynamic model of a full vehicle with eight degrees of freedom, shown in Figure 1, on the assumption that the vehicle has symmetrical weight with respect to X axis, and road inputs are isotropic ergodic processes, ignoring tire damping and any other vibration sources except for road roughness. The X axis points to the running direction of the vehicle, and the origin of the coordinate system is at the center of gravity of the vehicle body.

The differential equation of the above model can be easily derived from the Lagrange equation as,

$$[M]\{\ddot{Z}\} + [C]\{\dot{Z}\} + [K]\{Z\} = [P]\{I(t)\} \tag{1}$$

Where, $[M]$denotes the mass matrix,

$$[M] = \begin{bmatrix} m_s & 0 & 0 & 0 & 0 & 0 & 0 & 0 \\ 0 & m_B & 0 & 0 & 0 & 0 & 0 & 0 \\ 0 & 0 & J_y & 0 & 0 & 0 & 0 & 0 \\ 0 & 0 & 0 & J_x & 0 & 0 & 0 & 0 \\ 0 & 0 & 0 & 0 & m_{fl} & 0 & 0 & 0 \\ 0 & 0 & 0 & 0 & 0 & m_{fr} & 0 & 0 \\ 0 & 0 & 0 & 0 & 0 & 0 & m_r & 0 \\ 0 & 0 & 0 & 0 & 0 & 0 & 0 & J_{rq} \end{bmatrix}$$

$[C]$ denotes the damping matrix,

$$[C] = \begin{bmatrix} c_s & -c_s & -c_s l_4 & -c_s l_7 & 0 & 0 & 0 & 0 \\ -c & c_{22} & c_{23} & c_s l_7 & -c_f & -c_f & -2c_r & 0 \\ -c_s l_4 & c_{32} & c_{33} & c_s l_4 l_7 & -c_f l_1 & -c_f l_1 & 2c_r l_2 & 0 \\ -c_s l_7 & c_s l_7 & c_s l_4 l_7 & c_{44} & -c_f l_3 & c_f l_3 & 0 & -2c_r l_5^2 \\ 0 & -c_f & -c_f l_1 & -c_f l_3 & c_f & 0 & 0 & 0 \\ 0 & -c_f & -c_f l_1 & c_f l_3 & 0 & c_f & 0 & 0 \\ 0 & -2c_r & -2c_r l_2 & 0 & 0 & 0 & 2c_r & 0 \\ 0 & 0 & 0 & -2c_r l_3^2 & 0 & 0 & 0 & 2c, l_3^2 \end{bmatrix}$$

Here, $c_{22}=2c_f+2c_r+c_s$ $c_{23}=c_{32}=2c_f l_1-2c_r l_2+c_s l_4$
$c_{33}=2c_f l_1^2+2c_r l_2^2+c_s l_4^2$ $c_{44}=2c_f l_3^2+2c_r l_5^2+c_s l_7^2$

$[K]$ denotes the stiffness matrix,

$$[K] = \begin{bmatrix} k_s & -k_s & -k_s l_4 & -k_s l_7 & 0 & 0 & 0 & 0 \\ -k_s & k_{22} & k_{23} & k_s l_7 & -k_f & -k_f & -2k_r & 0 \\ -k_s l_4 & k_{32} & k_{33} & k_s l_4 l_7 & -k_f l_1 & -k_f l_1 & 2k_r l_2 & 0 \\ -k_s l_7 & k_s l_7 & k_s l_4 l_7 & k_{44} & -k_f l_3 & k_f l_3 & 0 & -2k_r l_5^2 \\ 0 & -k_f & -k_f l_1 & -k_f l_3 & k_{55} & 0 & 0 & 0 \\ 0 & -k_f & -k_f l_1 & k_f l_3 & 0 & k_{66} & 0 & 0 \\ 0 & -2k_r & -2k_r l_2 & 0 & 0 & 0 & k_{77} & 0 \\ 0 & 0 & 0 & -2k_r l_5^2 & 0 & 0 & 0 & 2k_{tr} l_8^2 \end{bmatrix}$$

Here, $k_{22}=2k_f+2k_r+k_s$ $k_{23}=k_{32}=2k_fl_1-2k_rl_2+k_sl_4$
$k_{33}=2k_fl_1^2+2k_rl_2^2+k_sl_4^2$ $k_{44}=2k_fl_3^2+2k_rl_5^2+k_sl_7^2$
$k_{55}=k_{66}=k_f+k_{tf}$ $k_{77}=2k_r+2k_{tr}$

$[P]$ denotes the transfer matrix from the road displacement vector, $\{I(t)\}$ to the force excitation vector,

$$[P]=\begin{bmatrix}0&0&0&0&k_{tf}&0&0&0\\0&0&0&0&0&0&k_{tr}&-k_{tr}l_8\\0&0&0&0&0&k_{tr}&0&0\\0&0&0&0&0&0&k_{tr}&k_{tr}l_8\end{bmatrix}^T \{I(t)\}=\begin{Bmatrix}I_1(t)\\I_2(t)\\I_3(t)\\I_4(t)\end{Bmatrix}$$

$\{\ddot{z}\}$, $\{\dot{z}\}$, $\{z\}$ are the system response vectors,

$$\{z\}=[z_s\ z_B\ \phi_B\ \theta_B\ z_{fl}\ z_{fr}\ z_r\ \theta_r]^T$$

Multiply both sides of Equation (1) by $[M]^{-1}$, and let $[A]=-[M]^{-1}[C]$, $[B]=-[M]^{-1}[K]$, $\{I'(t)\}=[M]^{-1}\{I(t)\}$, $\{x\}=[\{z\}\{\dot{z}\}]^T$ and $\{\dot{x}\}=[\{\dot{z}\}\{\ddot{z}\}]^T$, the system state equation can be expressed as,

$$\{\dot{x}\}_{16\times1}=\begin{bmatrix}[0]_{8\times8}&[E]_{8\times8}\\[B]_{8\times8}&[A]_{8\times8}\end{bmatrix}\{x\}_{16\times1}+\begin{Bmatrix}\{0\}_{8\times1}\\\{I'(t)\}_{8\times1}\end{Bmatrix} \quad (2)$$

Here $\{x\}$ is the state transfer vector with 16 dimension; $[E]$ is the unit matrix, and $\{I'(t)\}$ is the vector of force excitation, $\{I'(t)\}=[P]\{I(t)\}$.

2.2. Modeling of Correlated Four-wheel Road Roughness in the Time Domain

The filtered white-noise method was introduced in this paper. The essence of this method is to abstract some signals from an assumed system, in which a white-noise vector is regarded as an input. It can be described in mathematics as,

$$\{\dot{I}(t)\}=[A]\{I(t)\}+[B]\{W(t)\} \quad (3)$$

Where, $\{I(t)\}=[I_1(t), I_2(t), I_3(t), \ldots I_n(t)]^T$ is the road roughness vector; $\{W(t)\}=[W_1(t), W_2(t), W_3(t), \ldots$

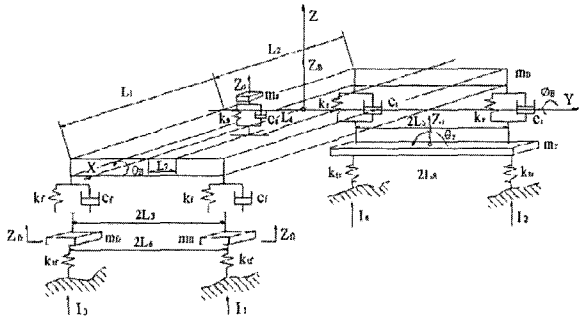

Figure 1. Dynamic model of a vehicle with 8 DOFs.

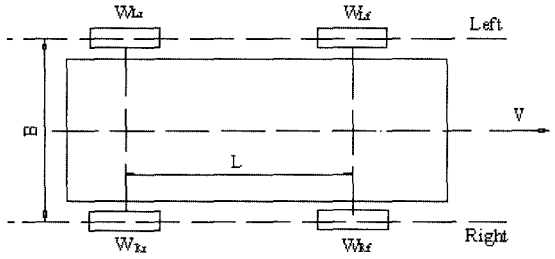

Figure 2. Sketch for a four-wheel vehicle.

$W_n(t)]^T$ is a row vector that consists of a white-noise series with a zero mean value each; t is time; $[A]$, $[B]$ are coefficient matrixes,

$$[A]=\begin{bmatrix}-aV&&0\\&-aV&\\&&\ddots\\0&&-aV\end{bmatrix}_{n\times n} \quad [B]=\begin{bmatrix}b&&0\\&b&\\&&\ddots\\0&&b\end{bmatrix}_{n\times n}$$

Here a, b are the constant coefficients, $a=2\pi n_0$, $b=2\pi\sqrt{G_0V}$, V is the vehicle velocity, n_0 is the cut-off frequency, $n_0=0.01$–0.1 c/m.; G_0 is the road coefficient, represent different grades of road. Note, if the vehicle velocity is constant, the assumed system described in Equation (3) is linear, and it may be feasible to study the correlation of road signals (system output) by studying the correlation of the white-noise series (system input).

For a four-wheel vehicle, the dimension n in the above model is 4, representing the left front wheel, right front wheel, left rear wheel and right rear wheel respectively. And the corresponding white-noise series is defined by W_{Lf}, W_{Rf}, W_{Lr}, W_{Rr} (see Figure 2). The road model for a four-wheel vehicle can be derived from the discussions of both the left-right tread correlation and the front-rear wheel correlation as follows.

2.2.1. Correlation between the left and right wheels

Assuming that the studied road surface is uniform, and the left and right wheel threads have isotropic statistic characteristics, the relationship between the transfer function and the coherence function of the left and the right wheels may be expressed as,

$$|H(\omega)|=coh(\omega) \quad (4)$$

Equation (4) is proved in the Appendix, according to the random vibration theory. Here the $coh(\omega)$ has been obtained from a road simulator, which is made by the MTS, by Changchun Automotive Research Institute of China, using a sample truck (CA141) at a forward speed of 50 km/h. Its expression is,

$$coh^2(\omega)=\begin{cases}1-0.45\omega & \omega\le2\pi rad/s\\0.1 & \omega>2\pi rad/s\end{cases} \quad (5)$$

According to modern control theory, the transfer function $W_{RL}(s)$ between W_{Lf} and W_{Rf} may be shown as the following form,

$$W_{RL}(s)=\frac{W_{Rf}(s)}{W_{Lf}(s)}=\frac{b_0+b_1s+b_2s^2+\cdots+b_ns^n}{a_0+a_1s+a_2s^2+\cdots+a_ns^n} \tag{6}$$

Thus,

$$|H(\omega)|=|W_{RL}(s)|=\frac{|b_0+b_1(j\omega)+b_2(j\omega)^2+\cdots+b_n(j\omega)^n|}{|a_0+a_1(j\omega)+a_2(j\omega)^2+\cdots+a_n(j\omega)^n|} \tag{7}$$

Where: $W_{Rf}(s)$, $W_{Lf}(s)$ are the Laplace transform of W_{Rf} and W_{Lf}, s is the Laplace operator, a_0, a_1, a_2, ..., a_n, b_0, b_1, b_2, ..., b_n are the coefficients, and can be carried out from Equations (4), (5) and (7) by optimization principles. The target function selected for optimization is,

$$\min \sum_{i=1}^{n} ||H(\omega_i)|-coh(\omega_i)| \tag{8}$$

And the constraint condition,

$$0 \le \omega_i \le 50 rad/s \tag{9a}$$

$$||H(\omega_i)|-coh(\omega_i)| < \varepsilon \tag{9b}$$

Where: ε is a small positive value.

In order to simplify the calculation, a third-order approximate formula is adopted, such as,

$$W_{RL}(s)=\frac{b_0+b_1s+b_2s^2+b_3s^3}{a_0+a_1s+a_2s^2+a_3s^3}=\frac{(b_0-b_2\omega_i^2)+(b_1\omega_i-b_3\omega_i^3)j}{(a_0-a_2\omega_i^2)+(a_1\omega_i-a_3\omega_i^3)j} \tag{10}$$

Let ε be equal to 0.05, and ω_i (i=1 2, 3, ..., n) equals 0 0.5, 1.0, ..., 50 in Equation (7). By the optimization program, the obtained coefficients are: a_0=3.2230, a_1=0.5900, a_2=0.0327, b_0=3.1815, b_1=0.2063, b_2=0.0108, a_3=b_3=0. Substituting them into Equation (10) gives the plots of the amplitude and phase as functions of the angular frequency (see Figure 3 and 4). A good agreement of the amplitudes can be seen from Figure 3. The curves indicate that the coefficients have enough precision to substitute the coherence function with the transfer function and the phase angle between the left and right wheel approach to zero. Dividing the numerator and denominator of Equation (10) by s^2 produces,

$$W_{RL}(s)=\frac{W_{Rf}(s)}{W_{Lf}(s)}=\frac{b_0s^{-2}+b_1s^{-1}+b_2}{a_0s^{-2}+a_1s^{-1}+a_2} \tag{11}$$

Setting an intermediate variable,

$$m(s)=\frac{W_{Lf}(s)}{a_0s^{-2}+a_1s^{-1}+a_2} \tag{12}$$

Then, $W_{Rf}(s)=m(s)\cdot(b_0s^{-2}+b_1s^{-1}+b_2)$ (13)

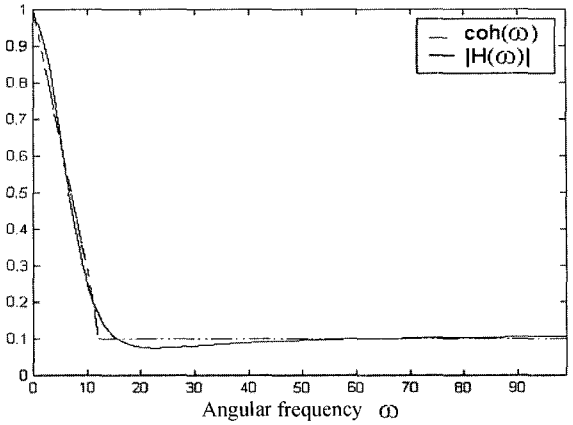

Figure 3. Amplitude versus angular frequency.

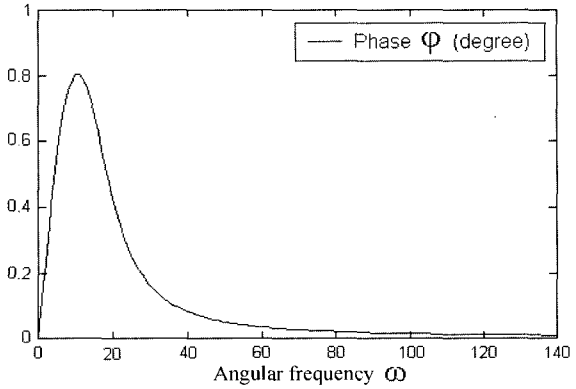

Figure 4. Phase versus angular frequency.

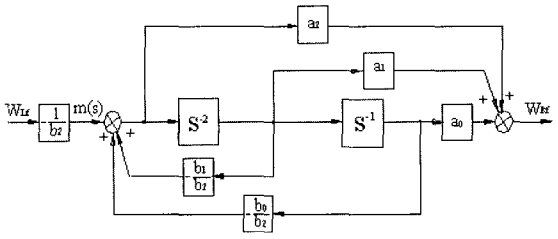

Figure 5. Systemic state-block diagram.

Therefore, the state equation of the correlation between the left and right wheels can be derived from Equations (12) and (13) as Equation (14), referring to the systemic state block diagram in Figure 5.

$$\begin{bmatrix}\dot{x}_1\\ \dot{x}_2\end{bmatrix}=\begin{bmatrix}0 & 1\\ -b_0/b_2 & -b_0/b_2\end{bmatrix}\begin{bmatrix}x_1\\ x_2\end{bmatrix}+\begin{bmatrix}0\\ 1/b_2\end{bmatrix}\cdot W_{Lf} \tag{14a}$$

$$W_{Rf}=\begin{bmatrix}a_0-a_2\frac{b_0}{b_2} & a_1-a_2\frac{b_1}{b_2}\end{bmatrix}\begin{bmatrix}x_1\\ x_2\end{bmatrix}+\frac{a_2}{b_2}\cdot W_{Lf} \tag{14b}$$

2.2.2. Correlation between the front and rear wheels
As is known, the input of the rear wheel must be later than that of the front wheel for a time difference T_h, $T_h=L/V$. Therefore, the relationship between W_{Lf} and W_{Lr} may be expressed as,

$$W_{Rf}(t)=W_{Lf1}(t-T_h)=W_{Lf}(t)e^{-j\omega Th} \tag{15}$$

Where, L, V, t represent the wheelbase, the forward velocity of the vehicle and time, respectively. Taking the Laplace transform of both sides of Equation (15) yields, $W_{fr}(s)=W_{Lr}(s)/W_{Lf}(s)=e^{-Ths}$.

Using the Pade approximate method supplies,

$$\frac{W_{Lr}(s)}{W_{Lf}(s)}=\frac{\sum_{i=1}^{N}(-1)^n P_n(T_h s)^n}{\sum_{i=1}^{N}P_n(T_h s)^n} \tag{16}$$

Here $P_n(n=1, 2, 3, ..., N)$ is a set of constant coefficients, $P_1=1/2$, $P_2=1/12$, ... Retaining the first three terms of the numerator and denominator, respectively,

$$\frac{W_{Lr}(s)}{W_{Lf}(s)}=\frac{1-\frac{T_h}{2}s+\frac{T_h^2}{12}s^2}{1-\frac{T_h}{2}+\frac{T_h^2}{12}s^2} \tag{17}$$

Following the same process as that in 2.2.1, the state equations concerning the hysteresis between the front and rear wheels becomes,

$$\begin{bmatrix}\dot{x}_3\\ \dot{x}_4\end{bmatrix}=\begin{bmatrix}0 & 1\\ 1 & -12/T_h^2\end{bmatrix}\begin{bmatrix}x_3\\ x_4\end{bmatrix}+\begin{bmatrix}0\\ 12/T_h^2\end{bmatrix}W_{Lf} \tag{18a}$$

$$W_{Lf}=[0\ -T_h]\begin{bmatrix}x_3\\ x_4\end{bmatrix}+W_{Lf} \tag{18b}$$

2.2.3. Correlation of four-wheel model of road roughness
After establishing the correlations of W_{Lf}, W_{Rf} and W_{Lr}, W_{Rr} may be gotten easily from Equations (13) and (17),

$$W_{Rr}=[0\ -T_h]\begin{bmatrix}x_3\\ x_4\end{bmatrix}+\begin{bmatrix}a_0-a_2\frac{b_0}{b_2} & a_1-a_0\frac{b_1}{b_2}\end{bmatrix}\begin{bmatrix}x_1\\ x_2\end{bmatrix} \tag{19}$$

The treatment of the above model equations is somewhat less straightforward. Let us pursue intuitive description further. Combining Equations (14), (18), (19) and substituting them into Equation (3), the final road model regarding the correlation characteristic of four wheels can be described as follows,

$$\{\dot{I}(t)\}=[A]\cdot\{I(t)\}+2\pi\sqrt{G_0V}\cdot[B_{wx}]\cdot\{x(t)\}+2\pi\sqrt{G_0V}\cdot[B_w]\cdot W_{Lf}(t) \tag{20a}$$

$$\{\dot{x}(t)\}=[A_x]\cdot\{x(t)\}+\{B_x\}\cdot W_{Lf}(t) \tag{20b}$$

Where: $\{x(t)\}$ is the state transfer vector; $\{B_w\}$, $\{B_x\}$, $\{B_{wx}\}$ and $[A_x]$ are the coefficient matrixes,

$$\{I(t)\}=\begin{Bmatrix}I_1(t)\\ I_2(t)\\ I_3(t)\\ I_4(t)\end{Bmatrix}\ \{x(t)\}=\begin{Bmatrix}x_1(t)\\ x_2(t)\\ x_3(t)\\ x_4(t)\end{Bmatrix}\ \{B_w\}=\begin{Bmatrix}1\\ a_2/b_2\\ 1\\ a_2/b_2\end{Bmatrix}\ \{B_x\}=\begin{Bmatrix}0\\ 1/b_2\\ 0\\ 12/T_h^2\end{Bmatrix}$$

$$[B_{wx}]=\begin{bmatrix}0 & 0 & 0 & 0\\ \left(a_0-a_2\frac{b_0}{b_2}\right) & \left(a_1-a_0\right)\frac{b_1}{b_2} & 0 & 0\\ 0 & 0 & 0 & -T_h\\ \left(a_0-a_2\frac{b_0}{b_2}\right) & \left(a_1-a_0\right)\frac{b_1}{b_2} & 0 & -T_h\end{bmatrix}\ [A_x]=\begin{bmatrix}0 & 1 & 0 & 0\\ -\frac{b_0}{b_2} & -\frac{b_1}{b_2} & 0 & 0\\ 0 & 0 & 0 & 1\\ 0 & 0 & -\frac{T_h^2}{12} & -\frac{6}{T_h}\end{bmatrix}$$

3. SIMULATION

A example, the most common nonstationary vibration processes, the accelerating and braking processes, of a passenger car were considered in this paper. The related parameter values used for the simulation study came from a bus named LQ91C10 (Lu, S. F., 1988), and are given in Table 1.

3.1. Simulation of Road Roughness
3.1.1. Verification of the proposed four-wheel road model
The computer simulation of the above road model was carried out in this paper, using the white-noise series W_{Lf} generated by computer as the model input, and considering the bus runs on a road of grade B

Table 1. Parameter values of the sample vehicle.

$m_B\,(kg)$	$J_y\,(kgm^2)$	$J_x\,(kgm^2)$	$m_{fl}\,(kg)$	$m_{fr}\,(kg)$	$m_r\,(kg)$	$J_{rq}\,(kgm^2)$	$m_s\,(kg)$
7408	37900	8919	205	205	1050	544.6	50
$k_{tf}\,(N/m)$	$k_{tr}\,(N/m)$	$k_f\,(N/m)$	$k_r\,(N/m)$	$k_s\,(N/m)$	$c_f\,(Ns/m)$	$c_r\,(Ns/m)$	$c_s\,(Ns/m)$
628000	1256000	177600	605800	22072	5020	15108	753
$l_1\,(m)$	$l_2\,(m)$	$l_3\,(m)$	$l_4\,(m)$	$l_5\,(m)$	$l_6\,(m)$	$l_7\,(m)$	$l_8\,(m)$
3.06	1.64	0.45	2.34	0.507	0.912	0.884	0.912

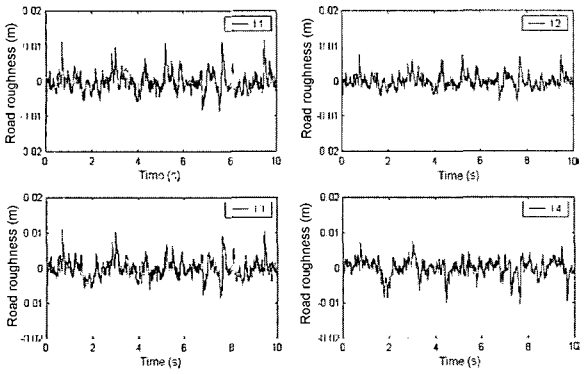

Figure 6. Time series of the road roughness.

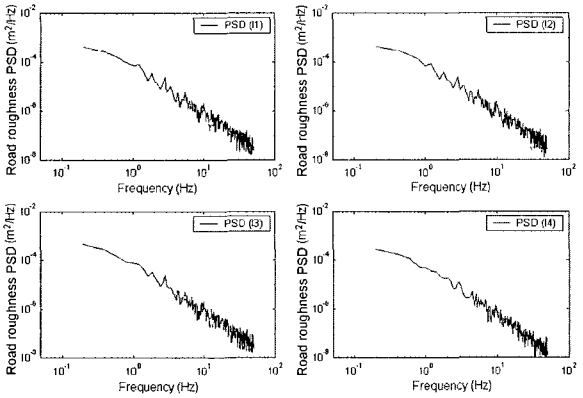

Figure 7. PSDs of the road roughness.

(G_0=6.4×10^{-5}) at 50 km/h. The time series of road elevations can be gotten by Runge-Kutta Method. $I_1(t)$, $I_2(t)$, $I_3(t)$ and $I_4(t)$ represent the road displacement input of left-front, right-front, left-rear and right-rear wheels, respectively. The simulation results are shown in Figure 6. In general, $I_1(t)$, $I_2(t)$, $I_3(t)$ and $I_4(t)$ have maximum amplitudes within the interval [-0.015m, +0.015m], and their power spectral densities (PSDs) shown in Figure 7 suggest that they also have the same energy distribution

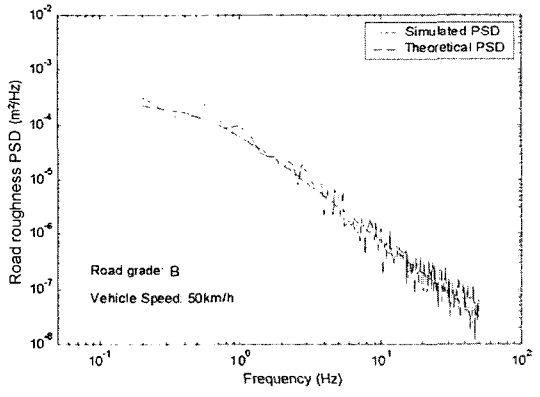

Figure 8. Comparison of the PSD of road roughness.

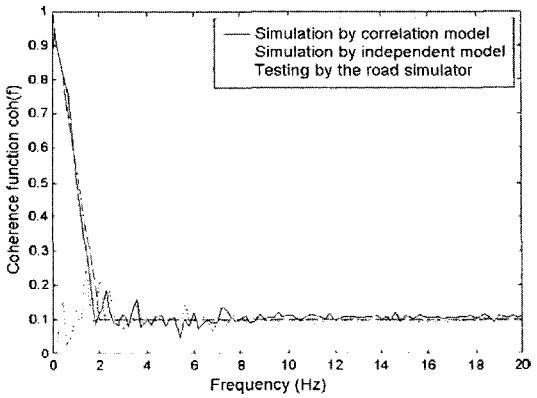

Figure 9. Comparison of the coherence function.

in the frequency domain.

From ISO/TC108/SC2N67, the theoretical power spectral density (PSD) of rough road in the frequency domain can be expressed as,

$$S_l(n)=S_l(n_0)\left(\frac{n}{n_0}\right)^{-2} \tag{21}$$

Where: $S_l(n)$ is the spatial frequency power spectral density; $S_l(n_0)$, a coefficient of road roughness, can be obtained from ISO/TC108/SC2N67 according to different road grades; n is spatial frequency; n_0 is the reference spatial frequency, n_0=0.01–0.1 *c/m*.

While a vehicle is running with constant speed, the relationship between vehicle traveling speed v, spatial frequency n and time frequency f is $f=nv$. Hence, Equation (21) becomes,

$$S_l(f)=S_l(n)/v=S_l(n_0)n_0^2v/f^2 \tag{22}$$

Based on Equation (22), the theoretical PSD of road roughness is carried out, see Figure 8. To verify simulated results, one of the simulated curves of the PSD was drawn on the same figure. The comparison shows that the simulated result is in agreement with the theoretical value.

The coherence function comparison between the simulation and testing are shown in Figure 9. The curves were calculated from the AR (p,0) method (Wang and Wu, 1987) and Equations (5), (A5) (see Appendix). The simulated road signal in Figure 6 has a similar coherence characteristic as the test data that came from the road simulator. For the independent AR (p, 0) road model, however, the coherence function values that should have been zero in theory when used in practice were around 0.1, and the peak value was not more than 0.25. Definitely, the correlation information was lost in the low-frequency scope. From Figure 7, the energy of road inputs were mainly distributed below 10 Hz, therefore,

the precision of road simulation must have been affected by the ignorance of the correlation in road modeling in the past, i.e., the correlated road model developed here is more accurate than the previous independent ones which have often been used as system inputs in vehicle vibration simulations.

Furthermore, the methods of sequence hypothesis inspection, autocorrelation function and χ^2 inspection were carried out, and the results show that the above road-roughness signals have stationarity, periodicity and normal distribution quality.

3.1.2. Simulation of nonstationary road roughness

Assuming that the sample vehicle starting at an initial speed v_0=0, first accelerating with a constant acceleration a_1=2.5 m/s^2 up to v_m=60 km/h, and then braking with another acceleration a_2=−4.5 m/s^2 down to v_f, therefore, the instantaneous vehicle speed at any time t may be expressed as,

$$V(t)=\begin{cases} v_0+a_1 t & 0<t<v_m/a_1 \\ v_m+a_2(t-v_m/a_1) & v_m/a_1<t<(v_m/a_1-v_m/a_2) \end{cases} \quad (23)$$

The above process is hereafter called "AAB" process.

Using the Runge-Kutta Method, the time series of road roughness may be calculated by substituting Equation (23) into Equation (20), and a set of calculation results of the road of grade C, for example, are shown in Figure 10. The calculation parameters are: the sample length is 2000 points; the road coefficient is G_0=2.56×10^{-4}; the resolutions of time and frequency are Δt=0.005s and Δf=0.1 Hz, respectively.

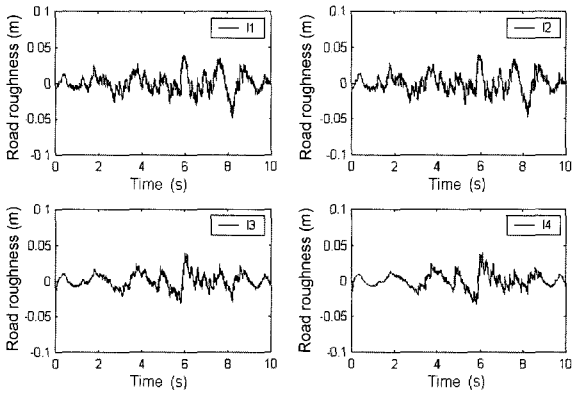

Figure 10. The road roughness of the four wheels during the "AAB" process (Grade C).

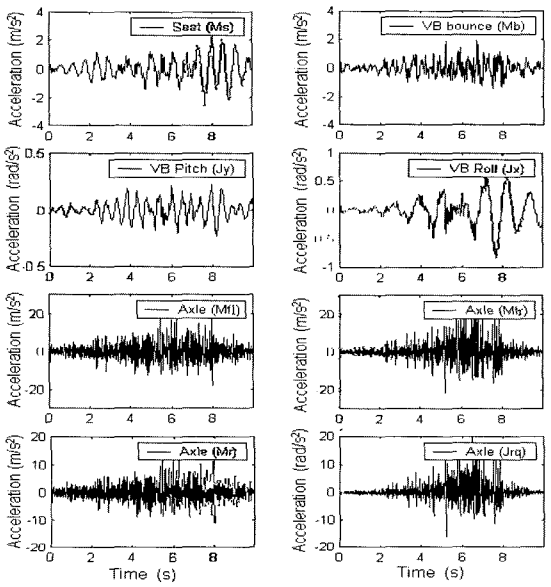

Figure 11. Acceleration responses of the vehicle during the "AAB" process.

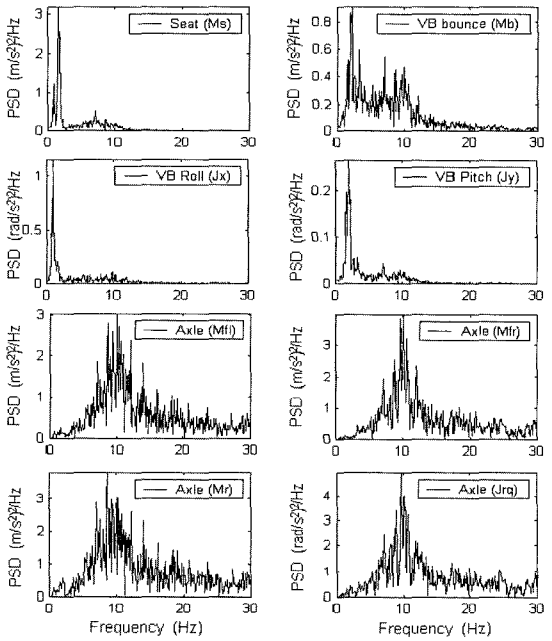

Figure 12. PSDs of the vehicle responses during the "AAB" process.

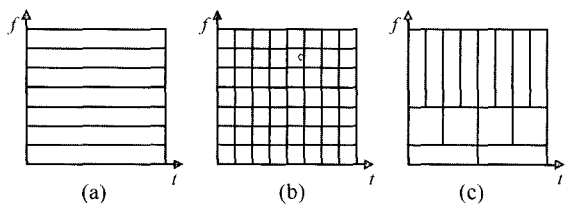

Figure 13. Comparison of the time-frequency resolution: (a) Fourier transform; (b) short-time Fourier transform; (c) wavelet transform.

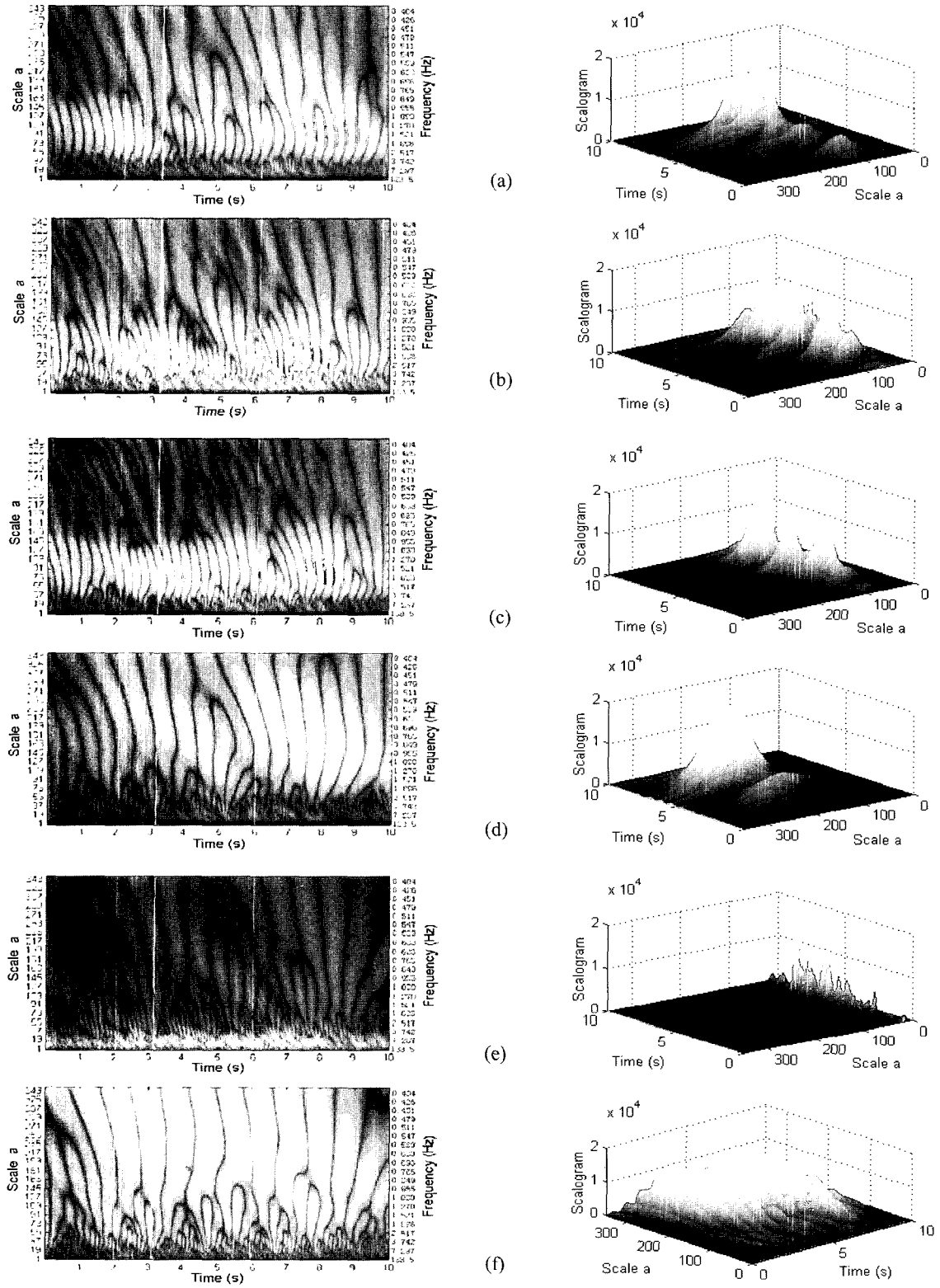

Figure 14. 2D and 3D scalograms result from CWT during the "AAB" process: (a) the vertical vibration of the driver seat; (b) (c) and (d) the vertical, pitch and roll vibrations of the vehicle body; (e) the vertical vibration of the front axle; (f) the road roughness of the right-rear wheel (I_2).

3.2. Simulation of Nonstationary Vehicle Responses

The Runge-Kutta Method can also be used to solve the vehicle response through Equation (2). Figure 11 shows the acceleration responses at positions of interest in Figure 1 during the "AAB" process, and Figure 12 in its corresponding PSDs. The same calculation parameters as those in the simulation of road roughness have been chosen. The validity of the above simulation procedure was verified by comparing the simulated results with the theoretically exact solutions (Zhang *et al.*, 2002).

4. WAVELET ANALYSIS (WA)

4.1. Trait of Wavelet Analysis

Wavelet analysis, which provides a perfect filtering characteristic, has been used extensively, in various fields of Mathematics, Science, and Engineering. Through the decomposition and reconstruction of a signal, wavelet analysis can be performed to determine the transient identity in the time-frequency domain, and therefore, is regarded as an effective approach for nonstationary data processing. The basic theory of wavelet analysis, including both of the continuous and the discrete versions, the conception of the scalogram, are briefly in the Appendix.

To illustrate the specialty of wavelet analysis, a comparison of time-frequency resolution between the conventional Fourier transform, short-time Fourier transform and the wavelet transform are shown in Figure 13. Apparently, the wavelet transform represents the next multi-resolution characteristic: a windowing technique with variable-sized regions. It allows the use of long intervals where we want more precise low-frequency information, and shorter regions where we want high-frequency information. This multi-resolution characteristic exactly meets the requirements of nonstationary signal processing. Therefore, wavelet analysis is selected in this paper to study nonstationary signals in vehicle vibration.

4.2. Wavelet Analysis of Simulation Signals

This paper executes the CWT and DWT by using the Mallat algorithm (or fast wavelet transform) in the Matlab toolbox. The Mallat algorithm, a very practical filtering algorithm, is in fact a classical scheme known as a two-channel subband coder in signal processing. The selected parameters for calculation are: the Daubechies wavelet with a filter length of seven (F_c=0.6923 Hz), the scaling factor a=1–350, i.e., the frequency range: 0.404–138.5 Hz.

Figure 14(a)–(f) shows the acceleration scalograms, which were obtained from the CWT, of the seat, vehicle body, axle and road roughness during the "AAB" process, respectively. And Table 2 lists the coordinate positions of the maximum vibration energy that appeared on the time-frequency map. As seen, the worst ride performance of the vehicle happened at 8s during the "AAB", and there was a 1.4s time delay in the vibrations transfer from road to the vehicle system. This might be attributed to the transfer characteristic of the suspension parts. In view of the frequency, the consistent frequency locations of the energy peaks have been adopted by comparing the results from the WT and FFT (see Table 2 and Figure 12).

From Figure 14(a)–(f), in the accelerating process, the vibration energies of the vehicle are getting bigger, moving, as well, to the higher-frequency area, their involved frequency bands are getting broader, and vice versa in the braking process. Figure 14(f) shows that the energy of the road roughness mainly distributed below 1.896 Hz, first rolls towards high-frequency with the increasing of the vehicle speed, and then converges to low-frequency after the peak velocity of the vehicle. As a rule, these phenomena of energy flow are transmitted to the other levels through the suspension system (see the texture in 2D scalogram of Figure 14(a)–(e)). Figure 14(c) shows that three increasing peaks fluctuate in the pitching vibration of the vehicle body. The rolling vibration of the vehicle body, however, is closely tied-up with the road inputs (see Figure 14(d)).

In view of the vehicle design, the ride comfort of the passenger seat is the most important to be considered. Comparing Figure 14(a)–(f), the energy of road excitation has been greatly restrained by the suspension system of the vehicle. However, the similar time-frequency traits can be seen in (a), (b) and (c), and the ride comfort of the seat deteriorates suddenly at a certain running speed. This means that the vertical and the pitching movement of the vehicle body have more effect on the vibration of seats than the rolling movement, and that the vibration energy of the vehicle body flowed into the resonance frequency region of the seat vibration system during the "AAB" process. As known from Table 2, the resonant frequency of the vehicle pitching (1.9 Hz), which is much closer to the seat system (1.6 Hz) than that of the vehicle bouncing (2.2 Hz), from the view of the frequency, offers more "contribution" to the seat vibration. This phenomenon of approximate overlap of resonance frequencies certainly should be avoided in

Table 2. Coordinate positions of the peaks of vibration energy.

Seat (vertical)	Vehicle body (bounce)	Vehicle body (pitch)	Vehicle body (roll)	Axle (vertical)	Road roughness
(8.0s, 1.6 Hz)	(7.8s, 2.2 Hz)	(8.2s, 1.9 Hz)	(7.8s, 0.9 Hz)	(8.0s, 10 Hz)	(6.6s, 0.8 Hz)

vehicle designs. Therefore, for improving the ride performance of a vehicle, designers have to consider, for instance, how to match the parameters of the front and rear suspensions, change the resonant frequency of the seat, mend the relevant mass, stiffness or damping, separate the resonance points of the seat and vehicle body, and so on.

As seen from Figure 14, wavelet transform provided the "energy flow" map of each examined point of interest for the vehicle transient vibration with some variable time-frequency resolutions. During the design stage of vehicles, it may be adopted to direct vehicle vibration system designs, especially for the transient working cases.

A point should be mentioned, to avoid the fair amount of calculation in CWT, a big sampling interval was used in the above study, and we could not find a clear view of the axle vibration in the frequency range of 7.287–138.5 Hz in Figure 14(e). As a supplement, DWT was further performed on the same axle vibration signal (cut-off frequency: 200 Hz), and the results show that the vibration energy is mostly focused on 6.25–12.5 Hz, which is similar to that in Figure 12.

5. CONCLUSION

This paper presented a set of approaches for solving the nonstationary vibration problem of road vehicles. Firstly, in the time domain, a new road model for four-wheel vehicles was derived by integrating all the correlation functions into a one-state equation. Comparing with the previous road models, it is the first time to introduce a correlation between the left and the right wheels, and build an integral time domain road model in theory. The simulated signals of the stationary road approach to the theoretical and tested curve in some references very well in both the time and the frequency domains. The comparison shows that the new road model is more accurate than the previous ones to simulate the real road in a time domain. Furthermore, based on a full-vehicle model with 8 DOFs, the nonstationary vibration process of starting, accelerating and braking (called AAB) of a passenger bus, as an example, was simulated in a time domain.

Finally, wavelet transform techniques including CWT and DWT were applied to analyze the simulated nonstationary signals. In contrast to the conventional Fourier transforms, wavelet transform can focus on any position on the time-frequency plane through dilating and translating its wavelet function, and get any detailed information of interest. The conclusion can be drawn that wavelet analysis may offer energy spectra information with respect to time and frequency by specifying the exact position of the transient characteristics of a nonstationary signal on a time-frequency map. In the study of nonstationary vehicle vibration, by comparing the scalograms of each vibration level and road input, we may know the status of energy flows, determine the source of vibrations, and moreover, accomplish the optimization of the parameters, etc.

It should be mentioned that the work done in this paper may be generalized to any other type of four-wheel vehicle running on any grade of road with some given speed functions or discrete-time series of running speed. In the design stage of a vehicle, these proposed methods might be used to simulate, analyze and forecast its ride performance, either in stationary or nonstationary cases. Therefore, it may be regarded as an accessorial tool for vehicle design, especially for active suspension design.

ACKNOWLEDGEMENTS–This work has been partially supported by the Korea Science and Engineering Foundation through the Research Center for Machine Parts and Materials Processing at the University of Ulsan.

APPENDIX

A. Relationship Between the Transfer Function and Coherence Function on Uniform Road Surfaces

For any vibration system, according to the Random Vibration Theory, the autocorrelation PSD $S_{XX}(\omega)$ of the system input, the transfer function $H(\omega)$ and the cross-correlation PSD $S_{XY}(\omega)$ between the system input and output can be shown as

$$S_{XY}(\omega)=H(\omega)S_{XX}(\omega) \tag{A1}$$

Where: $S_{XY}(\omega)$, $S_{XX}(\omega)$ are all the double-ended power spectral densities, and ω is the angular frequency.

Therefore, the cross-correlation PSD between the right and left wheels can be shown as,

$$S_{LR}(\omega)=H(\omega)S_{LL}(\omega) \tag{A2}$$

Here $S_{LR}(\omega)$ and $H(\omega)$ are the cross-correlation PSD and the transfer function between the right and left wheels; $S_{LL}(\omega)$ denotes the autocorrelation PSD of the left wheel. Multiplying both sides of the Equation 4 by 2, thus,

$$G_{LR}(\omega)=|H(\omega)|G_{LL}(\omega) \tag{A3}$$

$G_{LR}(\omega)$, $G_{LL}(\omega)$ are the single-ended power spectral densities. $G_{LR}(\omega)$ can also be shown as,

$$G_{LR}(\omega)=|G_{LR}(\omega)|e^{-j\phi LR(\omega)} \tag{A4}$$

Where $\phi_{LR}(\omega)$ is the angle of phase, j is the complex operator. From the definition of coherence function,

$$coh^2(w)=\frac{|G_{LR}(\omega)|^2}{G_{LL}(\omega)G_{RR}(\omega)} \tag{A5}$$

Suppose that the studied road surface is uniform, and that the wheel threads have isotropic statistic characteristics, i.e., $G_{LL}(\omega)=G_{RR}(\omega)$, $\phi_{LR}(\omega)=0$. Combining Equations (A3), (A4) and (A5), we can conclude that the amplitude of the transfer function is equal to the coherence function, i.e.,

$$|H(\omega)|=coh(w) \tag{A6}$$

B. Basic Theory of Wavelet Analysis (WA)

Wavelet analysis is used to decompose or reconstruct a signal using some wavelets. Wavelets are a family of orthogonal functions of type,

$$\Psi_{a,b}(t)=|a|^{-1/2}\psi[(t-b)/a]\ a,b\in R\ a\neq 0 \tag{B1}$$

generated from a "mother" wavelet function $\psi(t)$ by dilation and translation operations, which are governed by the scale factor a and shift factor b, respectively.

The CWT and its reconstruction version of a signal $f(t)\in L^2(R)$ are defined as,

$$W_f(a,b)=|a|^{-1/2}\int_{-\infty}^{+\infty} f(t)\psi^*[(t-b)/a]\ dt=\langle f(t),\Psi_{a,b}(t)\rangle \tag{B2}$$

$$f(t)=C_\Psi^{-1}\int_{-\infty}^{\infty}\int_{-\infty}^{\infty}[W_f(a,b)\Psi_{a,b}(t)/a^2]dadb \tag{B3}$$

Where, $\psi^*[(t-b)/a]$ is the complex conjugate of $\psi[(t-b)/a]$; $C_\Psi=\int_{\infty}|F_\Psi(\omega)|^2/|\omega|d\omega$, $F_\Psi(\omega)$ is the Fourier transform of $\Psi(t)$.

To avoid the fair amounts of calculation in CWT, a discrete version of CWT, a so-called dyadic DWT, is usually adopted in engineering practice. Let $a=2^{-j}$, $b=2^{-j}k$ ($j, k\in Z$), the Equations (B2) and (B3) may be rewritten in a dyadic discrete form,

$$W_f(a,b)=W_f(2^{-j},2^{-j}k)=2^j\int_{-\infty}^{+\infty}\psi(2^jt-k)f(t)dt \tag{B4}$$

$$f(t)=\sum_j\sum_k W_f(2^{-j},2^{-j}k)\psi(2^jt-k) \tag{B5}$$

Based on WT, A further conception of the scalogram is defined as the square of the decomposition coefficients of wavelet transform, i.e.,

$$SCAL_f(a,b)=|W_f(a,b)|^2 \tag{B6}$$

The relationship between the scaling factor and frequency can be described as,

$$F_a=F_c/(a\cdot\Delta t) \tag{B7}$$

Here F_a is the pseudo-frequency corresponding to the scaling factor a; F_c is the center frequency of a wavelet; Δt is the sampling period.

REFERENCES

Baydar, N. and Ball, A. (2001). A comparative study of acoustic and vibration signals in detection of gear failures using wigner-ville distribution. *Mechanical Systems and Signal Proceeding* **15, 6,** 1091–1107.

Brigham, E. O. (1988). *The Fast Fourier Transform and Its Applications.* Prentice-Hall. Englewood Cliffs. New Jersey.

Chen, F. S. (1998). *Wavelet Transform in Signal Processing Theory and Applications.* National Defense Publication of China, Beijing, China.

Daubechies, I. (1990). The wavelet transform, time frequency localization signal analysis. *IEEE Transactions on Information Theory,* **36,** 961–1005.

Dodds, C. J. and Robson, J. D. (1973). The description of road surface roughness. *Journal of Sound and Vibration,* **31,** 175–183.

Dokainish, M. A. and Elmadany, M. M. (1980). Random response of tractor-semitrailer system. *Veh. Sys. Dyn.,* **9,** 87–112.

Esmailzedeh, E. and Fahimi, F. (1997). Optimal adaptive active suspensions for a full car model. *Veh. Syst. Dyn.,* **27,** 89–107.

Gade, S. and Gram-Hansen, K. (1996). Non-stationary signal analysis using wavelet transform, short-time fourier transform and wigner-ville distribution, *B&K Technical Reviews*, **2**, Naerum, Denmark.

Hac, A. (1985). Suspension optimization of a 2-DOF vehicle model using stochastic optimal control technique. *Journal of Sound and Vibration* **100, 3,** 343–357.

Haday, M. B. A. and Crolla, D. A. (1989). Theoretical analysis of active suspension performance using a four-wheel vehicle model. *Proc. Ins. Eng. Journal of Automobile Engineering (D),* **203**, 125–135.

Hodges, C. H., Power, J. and Woodhouse, J. (1985). The use of the sonogram in structure acoustics and an application to the vibrations of cylindrical shells. *Journal of Sound and Vibration,* **101**, 203–218.

Lu, S. F. (1988). A study on ride performance simulation and experiment based on a 3D bus model. *Shanxi Auto*, **2**, 1–11.

Newland, D. E. (1984). *Random Vibrations and Spectral Analysis*. 2nd ed. Longman. New York.

Newland, D. E. (1994). Wavelet analysis of vibration, Part I: Theory and Part II: Wavelet Maps. ASME, *Journal of Vibration and Acoustics*, **116**, 409–425.

Renucci, M. P. (1976). A new approach to vehicle testing

by computer simulation of the vehicle response. *ISATA* **76, 1,** 68.

Shi, G. K. and Li, B. (1995). Determination of relative damping coefficients of automotive shock absorbers in design phase. *Chinese Automotive Engineering* **17, 6,** 367–373.

Thompson, A. G. (1984). Optimal and suboptimal linear active suspensions for road vehicles. *Veh. Syst. Dyn.*, **13**, 61–72.

Wang, B. Y. and Wu, Y. S. (1987). A new method for simulating road roughness by using AP (P, 0) series. *Journal of Wuhan Institute of Technology*, **2**, 60–88.

Welch, P. D. (1967). The use of FFT for the estimation of power spectral - a method based on time averaging over short modified period grams. *IEEE Trans*, AV-15.

Yoshimura, T. (1998). A semi-active suspension of passenger cars using fuzzy reasoning and the field testing. *Int. J. of Vehicle Design* **19, 2,** 150–165.

Yu, F. and Guo, K. H. (1998). Adaptive and self-tuning control of vehicle suspensions. *Chinese Automotive Engineering* **20, 4,** 193–200.

Zhang, H. X. (1986). Computer prediction of vehicle's ride quality. *Chinese Automotive Engineering* **8, 1,** 21–31.

Zhang, L. J., Lee, C. M. and Wang, Y. S. (2002). A study on nonstationary random vibration of a vehicle in time and frequency domains. *Int. J. Automotive Technology* **3, 3,** 101–109.